

Theoretical investigation of dual-wavelength packet signal storage with SOA-based dual loop optical buffer

Songnian Fu ^{a,*}, P. Shum ^a, Guo Ning ^a, Chongqing Wu ^b, Yajie Li ^b

^a Lightwave Technology Group, Network Technology Research Center (NTRC), 4th storey Research TechnoPlaza, Nanyang Technological University, 50 Nanyang Drive, Singapore 637553, Singapore

^b Institute of Optical Information, School of Science, Beijing Jiaotong University, Beijing 100081, PR China

Received 21 March 2007; received in revised form 28 June 2007; accepted 30 July 2007

Abstract

In this paper, we theoretically investigate the dual-wavelength packet signal storage in the semiconductor optical amplifier (SOA)-based dual-loop optical buffer (DLOB). The loadable function of the DLOB is implemented by the cross phase modulation induced by the SOA. The influence of the nonlinear phase shift on the chirp and distortion of the stored packet pulse is examined for the case of the dual-wavelength loadable operation. It is found that, when the overlapping area of the stored dual-wavelength pulse is less than half of the pulse width, the distortion of output pulse after storage is negligibly small. However the most severe distortion appears when the dual-wavelength pulses overlap completely. The peak power of output packet pulse is reduced by approximately 30%. The obtained results can provide helpful insight for experimental implementation.

© 2007 Elsevier B.V. All rights reserved.

Keywords: All-optical buffer; Semiconductor optical amplifier; Cross phase modulation; Chirp; Pulse distortion

1. Introduction

Dense wavelength-division multiplexing (DWDM) in conjunction with increasing line rates continues to allow the transport capacity to grow gracefully with multiterabit per second per fiber transport systems available today [1]. All optical packet switching (OPS) is a potential technique that has been introduced to fully utilize the bandwidth capacity provided by current optical network [2]. One of the key modules in an OPS system is an all-optical buffer [3], which provides a solution when two packets have a collision at the output port besides the various other networking tasks it performs. The performance of an optical buffer directly determines the structure and the switching efficiency of the OPS. The main function of an optical buffer is to introduce a delay to a pulse train passing through an optical material with acceptable waveform degradation.

The time for a pulse to pass through the optical material is known as the group delay, which is given by $T_g = L/v_g = Ln_g/c$. Here L is the length of the optical material, c is the speed of light in vacuum, and n_g is the group index of material, which is related to the refractive index n by $n_g = n + \omega dn/d\omega$, where ω is the radial frequency of the lightwave. Since the refractive index of the material $n(\omega)$ is frequency dependent, the group index of material can be varied by adjusting the material dispersion term $dn/d\omega$. Thus, to make the controllable delay to be as large as possible, one way is to make L as longer as possible, which is referred to as the fiber-loop type optical buffer. Another possible way is to slow down the group velocity of pulse, which is referred to as the slow-light type optical buffer. The slow-light type optical buffer can be achieved, for example, by using the large normal dispersion associated with a resonance of a bulk optical material and semiconductor devices. Previous researches on slow light usually make use of the electromagnetically-induced transparency (EIT) [4] or the coherent population oscillation

* Corresponding author. Tel.: +65 67904527; fax: +65 6792 6894.
E-mail address: songnian@ntu.edu.sg (S. Fu).

(CPO) [5], in which a narrow transparent window is created within an absorbing resonance by an intense coupling laser field. The slow light experiments in the optical fibers are also carried out via stimulated Brillouin scattering (SBS) [6], stimulated Raman scattering (SRS) [7] or Raman-assisted parametric amplification [8]. Though these results appear very promising, there is a trade-off between bandwidth and storage time. A number of technical challenges remain to be overcome before slow-light buffers become practical [9].

By now, many configurations have been proposed to solve the problems posed in the fiber-loop optical buffer. A 10 Gbps multi-wavelength fiber-loop optical buffer was reported relying on tunable filters and semiconductor optical amplifiers (SOA)-based wavelength converters. And the recirculating time is determined by the wavelength assignment to the optical signal [10]. Also several nonlinear recirculating optical buffers have been demonstrated with 10 Gbps terahertz optical asymmetric demultiplexer (TOAD) [11], SOA-assisted Sagnac switch [12], and 40 Gbps ultra-fast nonlinear interferometer (UNI) structure [13]. Besides SOA application, an optical buffer with a structure similar to a Fabry-Perot cavity based on the fiber parametric amplification was proposed. And a nonlinear optical loop mirror (NOLM) as an optical switch was applied to implement the ‘erase’ function [14]. Recently we have developed an SOA-based dual-loop optical buffer (DLOB) [15,16]. Compared with the single-loop optical buffer [17], the DLOB configuration is more compact. The recirculation function can be implemented without the use of additional components, such as a fiber mirror, fiber Bragg grating, or TOAD gate. With the help of a 3×3 coupler, the packet signal can be skillfully confined in the horizontal figure ‘8’ fiber loop. Due to the Sagnac interferometer arrangement, our proposed structure is stable. The required control power for the DLOB is of the order of 1 mW and no extra optical amplifier is needed to compensate for the power loss in the fiber loop.

Although DWDM technology allows the simultaneous propagation of more than one wavelength in a single fiber, most of current fiber-loop optical buffer configurations can be only operated with only one wavelength. As multi-wavelength packets enter all-optical buffer randomly, the pulses will overlap with each other in time domain and result in interaction during storage. Therefore the storage of multi-wavelength signals becomes more complicated than that of single wavelength signal. The objective of this paper is to extend the DLOB operation to dual-wavelength packet signal storage. After theoretical investigation, we derive the nonlinear phase difference influence on the dual-wavelength pulse chirp and distortion. The rest of this paper is organized as follows: Section 2 presents the principle of packet signals storage in DLOB. Section 3 discusses the influence of nonlinear phase difference on the pulse chirp and pulse distortion and conclusions are drawn in the final section.

2. Principle of DLOB

The DLOB configuration is shown in Fig. 1. The four side ports (port 1 to port 3, port 4 to port 6) of a 3×3 collinear coupler are connected accordingly to form a horizontal ‘8’ figure. Two polarization controllers (PCs) are used to bias the polarization of loops. Two wavelength division multiplexers (WDMs) and one SOA are employed to generate nonlinear phase difference (NPD) between signals propagating in the clockwise (CW) and counter-clockwise (CCW) directions of each loop, with the assistance of a control light. The SOA is placed offset from the centre of the optical fiber loop 1 and adjacent to the splicing point between the optical fiber loop 1 and the port 4 of the 3×3 collinear fiber coupler. The transfer matrix of the 3×3 collinear fiber coupler is given by

$$T = \begin{bmatrix} 1/2 & i\sqrt{2}/2 & -1/2 \\ i\sqrt{2}/2 & 0 & i\sqrt{2}/2 \\ -1/2 & i\sqrt{2}/2 & 1/2 \end{bmatrix} \quad (1)$$

A packet signal with electric field $E_{in}(t) = f(t)e^{-i\omega_0 t}$ at the angular frequency ω_0 is introduced at the port 2 of the 3×3 coupler. The output signals from this coupler can be expressed as

$$\begin{bmatrix} E_4 \\ E_5 \\ E_6 \end{bmatrix} = T \begin{bmatrix} E_1 \\ E_2 \\ E_3 \end{bmatrix} = \begin{bmatrix} i\frac{\sqrt{2}}{2}f(t) \\ 0 \\ i\frac{\sqrt{2}}{2}f(t) \end{bmatrix} \quad (2)$$

Then E_4 and E_6 will transmit in the CW and CCW direction respectively in the loop 1. If we import the optical control pulse synchronized with CW-traveling packet signal into the loop 1, the CW and CCW signals will experience different gain and nonlinear phase shift (NPS) due to the cross gain modulation (XGM) and the cross phase modulation (XPM), respectively. The CW-traveling signal will be amplified by the complex gain of SOA as $\bar{g}_{cw}(t) = g_{cw}(t)e^{-i\varphi_{cw}(t)}$, and likewise, the CCW-traveling signal will experience the gain as $\bar{g}_{ccw}(t) = g_{ccw}(t)e^{-i\varphi_{ccw}(t)}$, where $g_{cw}(t)$ and $g_{ccw}(t)$ are the SOA electric field gain for the CW and CCW directions, $\varphi_{cw}(t)$ and $\varphi_{ccw}(t)$ are the nonlinear phase shift for the CW and CCW directions, respectively. And the NPD $\Delta\varphi = \varphi_{cw} - \varphi_{ccw}$ and the field

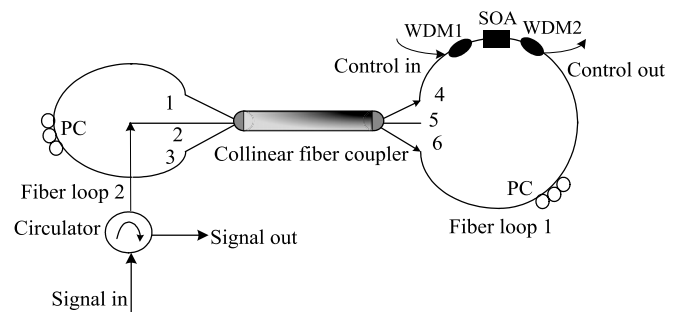


Fig. 1. The schematic diagram of dual-loop optical buffer. PC: polarization controller, WDM: wavelength division multiplexer.

gain ratio $\eta = g_{cw}/g_{ccw}$ for two different SOA states of saturation are coupled by [18]

$$\Delta\varphi = -\alpha \ln \left(\frac{g_{cw}}{g_{ccw}} \right) = -\alpha \ln(\eta) \quad (3)$$

Here α is the SOA linewidth enhancement factor. When the CW and CCW signals interfere at the coupler after transmission in loop 1, the output electrical fields can be expressed as

$$\begin{bmatrix} E_1 \\ E_2 \\ E_3 \end{bmatrix} = \mathbf{T} \begin{bmatrix} E_4 \\ E_5 \\ E_6 \end{bmatrix} = \frac{1}{2} E_{in}(t - t_1) |g_{ccw}| \sqrt{K} \exp(-j\varphi_{ccw}) \times \begin{bmatrix} j\frac{\sqrt{2}}{2} [1 - \exp(-\frac{\Delta\varphi}{\alpha}) \exp(-j\Delta\varphi)] \\ -[1 + \exp(-\frac{\Delta\varphi}{\alpha}) \exp(-j\Delta\varphi)] \\ -j\frac{\sqrt{2}}{2} [1 - \exp(-\frac{\Delta\varphi}{\alpha}) \exp(-j\Delta\varphi)] \end{bmatrix} \quad (4)$$

where K is the power attenuation coefficient of fiber loop 1, and t_1 is the group delay of loop 1. The value of the group delay of the standard single mode fiber is 5 ns per meter, if a group refractive index of 1.5 is assumed. For further investigations we are mainly interested in the output signal power for each 3×3 collinear port from Eq. (4), which is expressed as

$$\begin{bmatrix} P_1 \\ P_2 \\ P_3 \end{bmatrix} = \frac{1}{4} G_{ccw} K P_{in}(t - t_1) \times \begin{bmatrix} \frac{1}{2} [1 - 2 \exp(-\frac{\Delta\varphi}{\alpha}) \cos(\Delta\varphi) + \exp(-\frac{2\Delta\varphi}{\alpha})] \\ [1 + 2 \exp(-\frac{\Delta\varphi}{\alpha}) \cos(\Delta\varphi) + \exp(-\frac{2\Delta\varphi}{\alpha})] \\ \frac{1}{2} [1 - 2 \exp(-\frac{\Delta\varphi}{\alpha}) \cos(\Delta\varphi) + \exp(-\frac{2\Delta\varphi}{\alpha})] \end{bmatrix} \quad (5)$$

where $P_{in} = I^2(t - t_1)$ is the input packet signal power, and $G_{ccw} = g_{ccw}^2$ is the power gain in CW direction. From Eq. (5), it is obvious that port 1 and port 3 have the same out-

put power. In particular, considering $P_{in} = 1$ mW and $G_{ccw}K = 1$, we plot the relationship among P_1 , P_2 and NPD for various typical α values as shown in Fig. 2. First, when there is no NPD ($\Delta\varphi = 0$), the packet signals are combined and totally reflected to the port 2 of the coupler. Hence the amplified packet signals leave the DLOB directly after experiencing delay time of t_1 . All the input packets will undergo this delay regardless of whether they are to be buffered or not. However the CW-traveling packet signal will be induced with large nonlinear phase shift through the synchronous optical control pulse injection. Then the SOA can fully recover from the influence of the optical control pulse injection due to the offset of SOA position, so that the CCW-traveling packet signal is induced with a small nonlinear phase shift. By adjusting the SOA bias current to achieve $\Delta\varphi = \pi$, the packet signal will appear at port 1 and port 3 simultaneously, and only a very small packet signal will appear at port 2 due to the unbalanced gains G_{cw} and G_{ccw} . The power leakage at the port 2 is decreased with the growing of the SOA linewidth enhance factor. Then most of the packet signals will be re-circulated in the horizontal figure ‘8’ fiber loop, thus the packet storage is achieved. After several circulations, we can inject another control signal into the fiber loop 1, and acquire another NPD $\Delta\phi = \pi$ between two directional packet signals. The packet signal in the fiber loop 1 will then be exported from the DLOB. In this case the output electrical field from different ports of 3×3 collinear coupler is

$$\begin{bmatrix} E_1 \\ E_2 \\ E_3 \end{bmatrix} = \frac{1}{4} E_{in}(t - nt_d) \sqrt{G_{ccw}^{n+1} K^{n+1}} \exp(-2j\varphi_{ccw}) \times \begin{bmatrix} j\frac{\sqrt{2}}{2} [1 - \exp(-\frac{2\pi}{\alpha}) \exp(-2j\pi)] \\ -[1 - \exp(-\frac{\pi}{\alpha}) \exp(-j\pi)]^2 \\ -j\frac{\sqrt{2}}{2} [1 - \exp(-\frac{2\pi}{\alpha}) \exp(-2j\pi)] \end{bmatrix} \quad (6)$$

where t_d is the total delay of horizontal 8 figure fiber loop, and n is the number of circulations. From Eq. (6) it can be noted that most of packet signal leaves the DLOB and very little packet signal appears at the port 1 and port 3 of the 3×3 coupler. Finally the output power of stored packet P_{output} is calculated as

$$P_{output} = \frac{1}{16} P_{in}(t - nt_d) G_{ccw}^{n+1} K^{n+1} \left[1 + \exp\left(-\frac{\pi}{\alpha}\right) \right]^4 \quad (7)$$

3. Dual-wavelength operation

Firstly, the simulation setup for the dual-wavelength signal storage operation is described. Two laser modules at different wavelengths ($\lambda_1 = 1556.56$ nm, $\lambda_2 = 1557.36$ nm) are used as the packet signal light source, and another laser module at wavelength of 1553.4 nm is served as the control signal light source. The combined dual-wavelength light is introduced into a LiNbO3 Mach-Zehnder optical intensity modulator. Each packet with duration of 400 ns contains

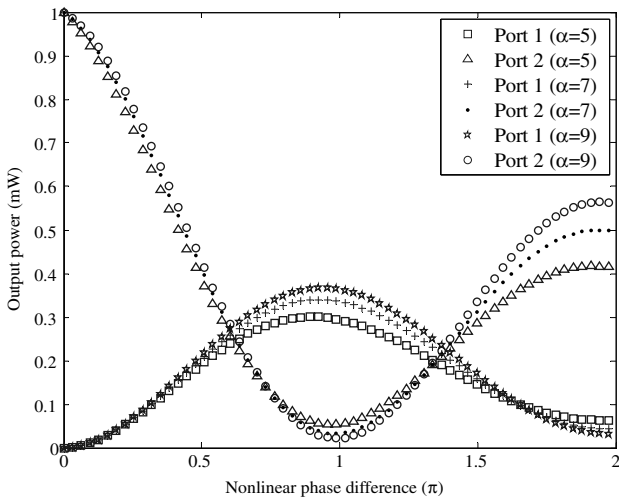


Fig. 2. The calculated output signal power at port 1 and port 2 with respect to the nonlinear phase difference for different α factors.

1000 bits $2^{15} - 1$ pseudorandom binary sequence (PRBS) at a bit rate of 2.5 GHz. According to the operation principle of the DLOB, the time interval between the loadable pulse and unloadable pulse should be an integral multiple of the group delay of whole fiber loop. Thus the optical control signal can be generated according to the format of packet signal. The peak power of the packet signal at each wavelength is $250 \mu\text{W}$ before entering into the DLOB, while the peak power of the optical control pulse is 2 mW. In our simulation, the lengths of the fiber loop 1 and loop 2 are 183 m and 117 m, respectively. The packet signal is released after one circle in the horizontal 8 figure fiber loop. Thus the total time delay t_d is $1.5 \mu\text{s}$ and n is equal to 1 in Eq. (7). A SOA with 1 mm length and 100 ps effective carrier lifetime is used in our simulation. A tunable optical filter is placed at the output port of the DLOB to differentiate the dual-wavelength packet signals. Then a photodetector (PD) with 12.5 GHz bandwidth is used to complete optical-electronic conversion. When the wavelength of the tunable filter at the PD side is set to λ_1 , the output waveform of stored λ_1 packet is obtained.

For the ease of discussion, it is assumed that the NPD from the SOA is mainly dependent on the peak power of the packet signal and the control pulse. Little XPM is generated between the dual-wavelength packet signals due to the weak injection power of the packet signal. Since the wavelength spacing of dual-wavelength signals is only 0.8 nm, it is assumed that the obtained NPD at different wavelength is almost the same when the peak power of dual-wavelength packet signal and control signal is fixed. The relatively slow SOA recovery time can cause unwanted pattern effects in the stored signal. Therefore the bit-rate of stored packet is maintained below 10 Gb/s, so that the distortion from pattern effect can be ignored in our later discussion. When the signal of dual-wavelength (λ_1 and λ_2) is launched into DLOB simultaneously, the pulses of two different wavelengths will overlap with each other in time domain. To further simplify our investigation, we refer the input pulse with Gaussian shape in wavelengths λ_1 and λ_2 as $P - 1$ and $P - 2$, respectively. Therefore the total power introduced into the DLOB is given by

$$P(T) = P_{P-1} + P_{P-2} = P_{\text{in}} \left\{ \exp \left[-\left(\frac{T}{T_0} \right)^2 \right] + \exp \left[-\left(\frac{T}{T_0} - (x+3) \right)^2 \right] \right\} \times (-3 \leq T/T_0 \leq 3, -3 \leq x \leq 3) \quad (8)$$

where T_0 is the half-width at the $1/e$ intensity point. For a Gaussian pulse, the full width at half maximum (FWHM) T_{FWHM} can be replaced with $1.665T_0$. It is assumed that $P - 1$ and $P - 2$ have the same peak power P_{in} and pulse width T_0 , and the overlapping region is demonstrated as the shadow area in Fig. 3, where x -axis is the normalized time scale T/T_0 , and y -axis denotes the normalized power of pulse. Note the cross term of the dual-wavelength signal

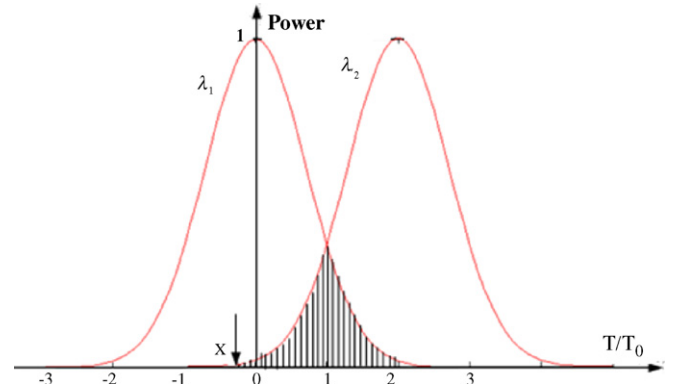


Fig. 3. Representation of overlapping area between dual-wavelength packet pulses.

is ignored in Eq. (8) due to the presence of a tunable optical filter. Now the overlapping area can be depicted by the value of x ($-3 \leq x \leq 3$). When $x = 3$, it means that $P - 1$ and $P - 2$ are detached completely, no overlapping takes place. However $x = 0$ means that only half width of $P1$ or $P2$ is overlapping, and $P - 1$ and $P - 2$ are overlapping completely under condition, $x = -3$. The smaller x is, the bigger area of overlapping is. The SOA power gain for the CW and CCW directions under the control pulse injection, G_{cw} and G_{ccw} , respectively, can be described as [19]

$$G_{\text{cw}} = G_0 \exp \left[\left(1 - G_{\text{cw}} \right) \frac{P_{\text{cw}} + P_c}{P_s} \right] \quad (9)$$

$$G_{\text{ccw}} = G_0 \exp \left[\left(1 - G_{\text{ccw}} \right) \frac{P_{\text{ccw}}}{P_s} \right] \quad (10)$$

where G_0 is the SOA small signal gain, P_s is the SOA saturation power in active region, P_c is the peak power of optical control pulse, P_{cw} and P_{ccw} are the peak power of packet signals in the CW and CCW direction, respectively and there is $P_{\text{cw}} = P_{\text{ccw}} = \frac{1}{2}P(T)$.

Then with Eqs. (3), (9), (10), we can obtain the NPD distribution $\Delta\varphi_{\lambda 1}(T)$ of $P - 1$ considering the influence of $P - 2$.

$$\Delta\varphi_{\lambda 1}(T) = \frac{\alpha}{2} \left\{ [1 - G_{\text{ccw}}(T)] \frac{\frac{1}{2}P_{\text{in}} \left\{ \exp \left[-\left(\frac{T}{T_0} \right)^2 \right] + \exp \left[-\left(\frac{T}{T_0} - (x+3) \right)^2 \right] \right\}}{P_s} - [1 - G_{\text{cw}}(T)] \frac{\frac{1}{2}P_{\text{in}} \left\{ \exp \left[-\left(\frac{T}{T_0} \right)^2 \right] + \exp \left[-\left(\frac{T}{T_0} - (x+3) \right)^2 \right] \right\} + P_c}{P_s} \right\} \times (-3 \leq x \leq 3) \quad (11)$$

$\Delta\varphi_{\lambda 2}(T)$ and $\Delta\varphi_{\lambda 1}(T)$ are symmetrically distributed along $T/T_0 = 0$ in our investigation, that is $\Delta\varphi_{\lambda 1}(T) = \Delta\varphi_{\lambda 2}(-T)$. Therefore we only discuss $P - 1$ in the following section. In our simulation, the SOA α is 5.31, G_0 is 18.3 dB, and P_s is 10.06 dBm. When the peak power P_{in} is $250 \mu\text{W}$, the requisite peak power of optical control pulse P_c is 2 mW to obtain $\Delta\phi = \pi$. Considering different x value, we plot the calculated NPD distribution with respect to pulse shape

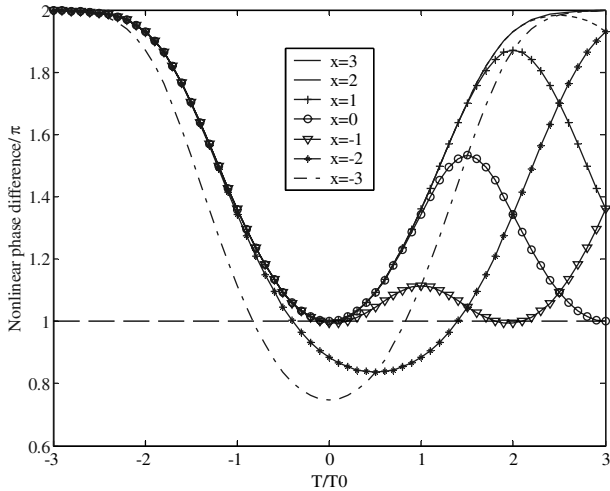


Fig. 4. The calculated nonlinear phase difference distribution as a function of T/T_0 with respect to the different x value.

in Fig. 4. It is quite interesting to find that when $P - 2$ does not overlap with $P - 1$ ($x = 3$), the NPD in midpoint of pulse ($T/T_0 = 0$) is just π , while the NPD deviates from π at the leading and trailing edges of packet pulse. Because the pulse width of control signal is selected to cover the whole of packet signal including lots of pulses, as a result the packet pulse can't obtain the same NPD at the different part of pulse with the constant power injection of optical control pulse. We also observe that, compared with the no overlapping situation, the reduced x leads to larger decrease of NPD, and the deviation mainly occurs in the trailing edge of pulse ($T/T_0 > 0$), the leading edge ($T/T_0 < 0$) has little deviation of NPD. When $P - 2$ is overlapping with $P - 1$ completely ($x = -3$), the NPD deviation distributes across the whole region of pulse. Since the dependence of $\Delta\varphi_{\lambda 1}$ on time could be expressed by chirp $\delta\omega_{\lambda 1}(T)$, taking the differential of Eq. (11), we can derive the chirp distribution of $P - 1$.

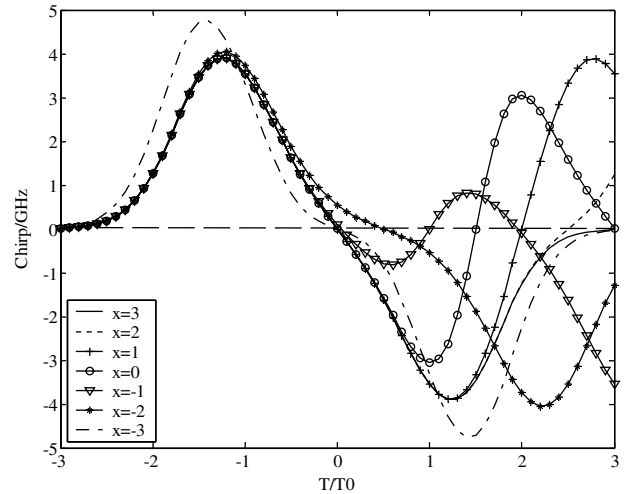


Fig. 5. The calculated chirp distribution as a function of T/T_0 with respect to the different x value.

Considering $T_0 = 400$ ps and different x value, the calculated $\delta\omega_{\lambda 1}(T)$ distribution with the respect to the pulse shape is plotted in Fig. 5. It is observed that, the chirp is always positive, i.e. blue-shifted, in the leading edge ($T/T_0 < 0$), regardless of the value of x . However in the trailing edge of pulse ($T/T_0 > 0$), the chirp keeps negative, i.e. red-shifted, only at $x = 3, -3$. While $x = 2, 1, 0, -1, -2$, both red-shifted and blue-shifted chirp appear. When pulse width T_0 is replaced with other values, we conclude that the whole evolution trend of $\delta\varphi_{\lambda 1}(T)$ is the same, and only the corresponding maximum value of $\delta\varphi_{\lambda 1}(T)$ is different. In order to investigate the pulse distortion after storage, we derive the waveform of output $P - 1$ considering the NPD distribution in Eq. (11)

$$\delta\omega_{\lambda 1}(T) = -\frac{\partial\Delta\varphi_{\lambda 1}(T)}{\partial T} = \frac{\alpha}{2} \left\{ \frac{[G_{cw}(T)-1]\frac{P_{in}}{T_0 P_s} \left\{ \left(\frac{T}{T_0}\right) \exp\left[-\left(\frac{T}{T_0}\right)^2\right] + \left[\frac{T}{T_0}-(x+3)\right] \exp\left[-\left(\frac{T}{T_0}-(x+3)\right)^2\right] \right\}}{\frac{1}{2}P_{in} \left\{ \exp\left[-\left(\frac{T}{T_0}\right)^2\right] + \exp\left[-\left(\frac{T}{T_0}-(x+3)\right)^2\right] \right\} + P_c} \exp\left\{ \frac{1}{2}P_{in} \left\{ \exp\left[-\left(\frac{T}{T_0}\right)^2\right] + \exp\left[-\left(\frac{T}{T_0}-(x+3)\right)^2\right] \right\} + P_c} \right\} [1-G_{cw}(T)]}{[G_{ccw}(T)-1]\frac{P_{in}}{T_0 P_s} \left\{ \left(\frac{T}{T_0}\right) \exp\left[-\left(\frac{T}{T_0}\right)^2\right] + \left[\frac{T}{T_0}-(x+3)\right] \exp\left[-\left(\frac{T}{T_0}-(x+3)\right)^2\right] \right\}} \exp\left\{ \frac{1}{2}P_{in} \left\{ \exp\left[-\left(\frac{T}{T_0}\right)^2\right] + \exp\left[-\left(\frac{T}{T_0}-(x+3)\right)^2\right] \right\} \right\} [1-G_{ccw}(T)]} \right\} \quad (12)$$

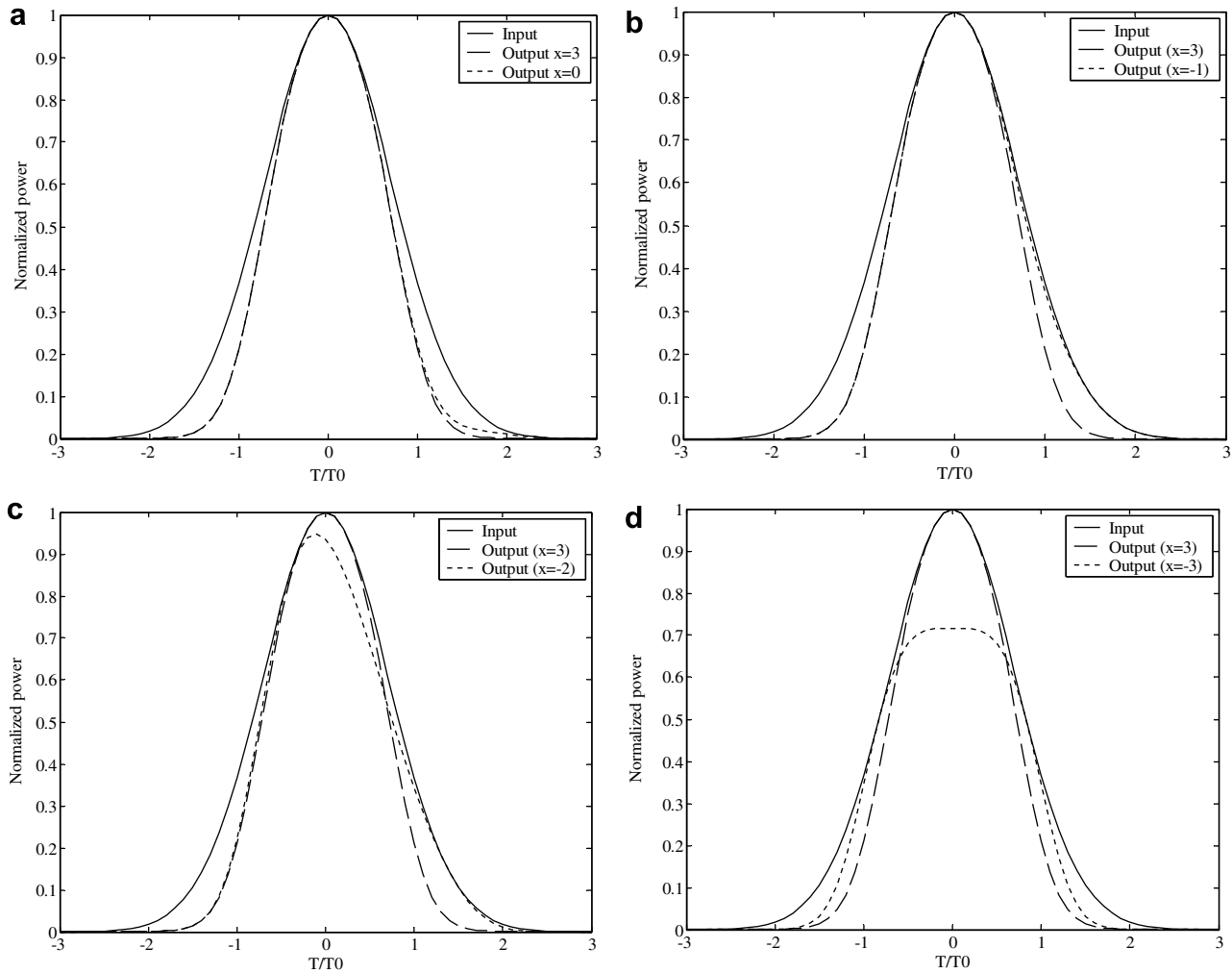


Fig. 6. The theoretical pulse distortion of the $P - 1$ packet with respect to the different x value. The input Gaussian pulse (solid line) and output shape of $P - 1$ when $P - 2$ does not overlap with $P - 1$, i.e. $x = 3$, (dashed line) are also shown in comparison. The dotted line is output shape of $P - 1$ when $P - 2$ is overlapped with $P - 1$ to some extent. (a) Output shape of $P - 1$ when $x = 0$. (b) Output shape of $P - 1$ when $x = -1$. (c) Output shape of $P - 1$ when $x = -2$. (d) Output shape of $P - 1$ when $x = -3$.

$$\begin{aligned}
 P_{\text{output},\lambda_1}(T) &= \frac{1}{16} G_{\text{ccw}}^{n+1} K^{n+1} P_{\text{in}} \exp\left[-\left(\frac{T}{T_0}\right)^2\right] (t - nt_d) \\
 &\times \left\{ \left[\left(1 - 2\exp\left(-\frac{\Delta\varphi_{\lambda_1}(T)}{\alpha}\right) \cos\Delta\varphi_{\lambda_1}(T) + \exp\left(-\frac{2\Delta\varphi_{\lambda_1}(T)}{\alpha}\right) \cos 2\Delta\varphi_{\lambda_1}(T) \right)^2 \right. \right. \\
 &\left. \left. + \left[\exp\left(-\frac{2\Delta\varphi_{\lambda_1}(T)}{\alpha}\right) \sin 2\Delta\varphi_{\lambda_1}(T) - 2\exp\left(-\frac{\Delta\varphi_{\lambda_1}(T)}{\alpha}\right) \sin\Delta\varphi_{\lambda_1}(T) \right]^2 \right\} \quad (13)
 \end{aligned}$$

Now using Eqs. (11) and (13) we can calculate precisely the output pulse power $P_{\text{output},\lambda_1}(T)$. The input and output pulse shape of the DLOB can be compared clearly in Fig. 6, where the solid line denotes the input shape of $P - 1$, dashed line is the output shape of $P - 1$ when $P - 2$ has no overlapping with $P - 1$, and dotted line is output shape of $P - 1$ when $P - 2$ is overlapped with $P - 1$ to some extent. When there is no overlapping ($x = 3$) and half of pulse is overlapped ($x = 0$), the pulse shapes of input and output are demonstrated in Fig. 6a. Comparing with the in-

put pulse shape, we can see that the output pulse is compressed regardless of the overlapping of dual-wavelength signals. Because the NPD at the pulse leading and trailing edges deviates from ideal value π as Fig. 4 shows, so output power of these parts deviate from their original value. Compared with the case in which $x = 3$, only the output power of trailing edge of $P - 1$ is enhanced slightly when $P - 2$ is overlapped with $P - 1$. When the overlapping area is increased as $x = -1$, the output shape of $P - 1$ is shown in Fig. 6b, the rising edge still covers the output curve of $x = 3$, but the trailing edge is departed with the output curve of $x = 3$ and very closed to the input pulse curve. When x value is further reduced to -2 , we note that output peak power of $P - 1$ is decreased and its peak position moves forward in Fig. 6c. The most severe pulse distortion occurs when $P - 2$ overlaps with $P - 1$ completely ($x = -3$), and the output shape of $P - 1$ is shown in Fig. 6d. We can observe that output peak power of $P - 1$ is reduced approximately by 30%. Finally we can conclude

that, when the overlapping area of dual-wavelength pulse is less than half of pulse width, the distortion of output pulse after storage is negligibly small. However the most severe distortion with 30% peak power reduction appears, when the dual-wavelength pulses overlap completely.

4. Conclusion

In this paper, we theoretically investigate the dual-wavelength packet signal storage in SOA-based dual-loop optical buffer. After theoretical investigation, we find that when the dual-wavelength signal is stored, the NPD at different parts of pulse will deviate from ideal value π because of dual-wavelength signal overlapping. This NPD deviation will lead to the pulse distortion after storage. We present the relationship between the NPD, chirp and the stored pulse distortion with respect to the extent of dual-wavelength pulse overlapping. When the overlapping area is less than half of pulse width, the pulse distortion is so little that it can be ignored. When the packet pulses of dual-wavelength overlap completely, the pulse distortion, which results in approximately 30% peak power reduction, is the most severe. The theoretical investigation provides helpful insight for experimental implementation.

Acknowledgements

This work is partially supported by the project M47040039 of Agency for Science, Technology and Research, Singapore, and partially supported by Open Fund of Key Laboratory of OCLT, BUPT, Ministry of Education, P. R. China. The authors acknowledge the valuable comments from the anonymous reviewers.

References

- [1] Hiro Suzuki, Masamichi Fujiwara, Katsumi Iwatsuki, J. Lightwave Technol. 24 (5) (2006) 1998.
- [2] K.E. Zoiros, M. Kalyvas, T. Houbavlis, J. Commun. Network 23 (2003) 124.
- [3] K.E. Zoiros, T. Houbavlis, M. Kalyvas, Opt. Quant. Electron. 36 (11) (2004) 1005.
- [4] A.V. Turukhin, V.S. Sudarshanam, M.S. Shahriar, J.A. Musser, Phys. Rev. Lett. 88 (2002) 023602.
- [5] Matthew S. Bigelow, Nick N. Lepeshkin, Robert W. Boyd, Phys. Rev. Lett. 90 (2003) 023602.
- [6] Zhaoming Zhu, Andrew M.C. Dawes, Daniel J. Gauthier, 12-GHz-bandwidth SBS slow light in optical fibers, in: Proc. OFC., PDP1, 2006.
- [7] Jay E. Sharping, Yoshitomo Okawachi, Alexander L. Gaeta, Opt. Express. 13 (16) (2005) 6092.
- [8] David Dahan, Gadi Eisenstein, Opt. Express. 13 (16) (2005) 6234.
- [9] R.S. Tucker, Pei-Cheng Ku, C.J. Chang-Hasnain, J. Lightwave Technol. 23 (12) (2005) 4046.
- [10] S.L. Danielsen, B. Mikkelsen, C. Joergensen, T. Durhuus, Photon. Technol. Lett. 8 (3) (1996) 434.
- [11] A.J. Poustie, K.J. Blow, R.J. Manning, Opt. Commun. 140 (1997) 184.
- [12] T. Houbavlis, K.E. Zoiros, Optik-Int. J. Light Electron Optics 114 (7) (2003) 322.
- [13] K.L. Hall, J.P. Donnelly, S.H. Groves, C.I. Fennelly, R.J. Bailey, A. Napoleone, Opt. Lett. 22 (1997) 1479.
- [14] A. Agarwal, W. Lijun, Yikai Su, P. Kumar, J. Lightwave Technol. 23 (7) (2005) 2229.
- [15] Aiming Liu, Chongqing Wu, Yandong Gong, P. Shum, Photon. Technol. Lett. 16 (9) (2004) 2129.
- [16] Songnian Fu, P. Shum, Liren Zhang, Chongqing Wu, A.M. Liu, J. Lightwave Technol. 24 (7) (2006) 2768.
- [17] Glenn D. Bartolini, Darwin K. Serkland, Prem Kumar, William L. Kath, IEEE Photon. Technol. Lett. 9 (7) (1997) 1020.
- [18] M. Eiselt, W. Pieper, H.G. Weber, J. Lightwave Technol. 13 (10) (1995) 2099.
- [19] Govind P. Agrawal, N. Anders Olsson, J. Quant. Electron. 25 (11) (1989) 2297.